



Construction and fine tuning of host-guest doping systems and the underlying mechanism of room temperature phosphorescence

Jianfeng Jiang^{a,1}, Jiaqi Liu^{b,1}, Chenwei Hu^b, Yongtao Wang^{a,*}, Lei Ma^{b,**}

^a Guangxi Key Laboratory of Electrochemical and Magneto-chemical Function Material, College of Chemistry and Bioengineering, Guilin University of Technology, Guilin, 541004, China

^b Tianjin International Center for Nanoparticles and Nanosystem, Tianjin University, Tianjin, 300072, China

ARTICLE INFO

Keywords:

Room-temperature phosphorescence
Host-guest doping
Carbazole derivatives
Imidazopyridine derivatives

ABSTRACT

To obtain ultralong and efficient pure organic room temperature phosphorescent materials, as well as explore the intrinsic mechanisms affecting the phosphorescence performance of host-guest doping systems, two carbazole derivatives with the same molecular structure, named as L-CzIPCN and CzIPCN, were prepared by using carbazole synthesized in the laboratory and commercial carbazole. By choosing L-CzIPCN/CzIPCN and poly-methyl methacrylate (PMMA)/polyvinyl alcohol (PVA)/benzophenone derivatives (BP, F-BP, Br-BP, and DF-BP) as the guest and host respectively, a series of new doping systems were constructed, and optimized by tuning doping ratios between host and guest materials. Among of them, F-BP/L-CzIPCN shows the longest room temperature phosphorescence (RTP) lifetime (501.23 ms), with RTP quantum yield of 31.19 %, followed by 0.2 % L-CzIPCN@PVA film (221.66 ms, 5.86 %) and 0.2 % L-CzIPCN@PMMA film (102.73 ms, 4.28 %) respectively. Moreover, L-CzIPCN displays different RTP spectra in diverse hosts, with dual-band RTP emission at 550 nm and 600 nm in benzophenone derivatives, but single RTP emission maxima in PMMA films, as well as a main emission peak at 470–510 nm and a shoulder peak at 550–590 nm in PVA films. The UV–Vis absorption spectra, fluorescence and phosphorescence spectra, and theoretical calculations indicate that RTP comes from the guest monomers in benzophenone derivatives/L-CzIPCN doping systems, with local triple characteristics, and host materials with large dipole moment, appropriate T_1 energy level, and small energy gap between S_1 and T_1 contribute to improving RTP performance of the doping systems. Based on the excellent luminescence and different RTP lifetimes of the doping systems, some high-level anti-counterfeiting, and information encryption patterns were successfully constructed.

1. Introduction

Purely organic room-temperature phosphorescence (PORTP) materials have significant research value in anti-counterfeiting, biological imaging and sensing due to unique characteristics such as large Stokes shift, long phosphorescence lifetime and high sensitivity to the environment [1–3]. However, highly efficient PORTP materials are difficult to construct due to weak intersystem spin-orbit coupling (SOC) and rapid non-radiative transition of triplet excitons (T_n) [4–8]. Currently, boosting intersystem transitions (ISC) and suppressing non radiative deactivation of triplet excitons have become two important means of obtaining organic ultralong room temperature phosphorescence (URTP)

materials [9,10]. Foregone studies showed that twisted donor- π -acceptors (D- π -A) luminogens could narrow the energy gap (ΔE_{ST}) between the lowest singlet state (S_1) and triplet state (T_1), and thereby boosted ISC and generation of more triplet excitons, while introducing heteroatom, heavy halogen atom and carbonyl group contributed to enhance SOC between singlet state and triplet state [11–13]. To stabilize the triplet excitons and suppress non-radiative energy loss induced by oxygen and molecular motion, crystallization and host-guest doping have been widely used [14–17]. Compared with crystallization, host-guest doping has attracted more extensive attention due to large area machinability, low cost, wide molecular structure, and controllable phosphorescence properties [18–23].

* Corresponding author.

** Corresponding author.

E-mail addresses: wyt_shzu@163.com (Y. Wang), lei.ma@tju.edu.cn (L. Ma).

¹ Jianfeng Jiang and Jiaqi Liu contributed equally.

Notably, RTP properties of host-guest doping not only depends on the doping modes such as grinding, eutectic and co-melting, but also depends on the intermolecular interaction, stacking and arrangement mode, and the excited state energy level between host and guest materials [24–31]. For examples, Liu et al. found that trace 1H-benzo[f]indole (Bd) in commercial carbazole played an important role in realization of RTP, which was attributed to formation of photo-induced charge-separated states [32]. Dong et al. found that the synergistic effect of the host and guest electronic structures could enhance RTP emission and lengthen RTP lifetime, in other words, D- π -A type host material corresponded to the A- π -A type guest material, and the A- π -A type guest material corresponded to the D- π -A type host material [33]. Huang et al. confirmed that the doping system showed stronger RTP when guest materials were dispersed in the host materials in the form of clusters [34]. Chen et al. developed a series of deep-blue RTP materials based on efficient energy transfer from host to guest via a Dexter energy transfer process [35]. Dong et al. constructed ultralong RTP materials by host materials reducing ΔE_{ST} of guest materials [36]. Obviously, the host-guest doping systems lack a unified theoretical explanation, which are not conducive to form efficient molecular design rules [37]. Presently, the host-guest RTP system is still in its infancy, and the underlying internal mechanisms still need to be further clarified by the selection and construction of more host and guest materials [38,39].

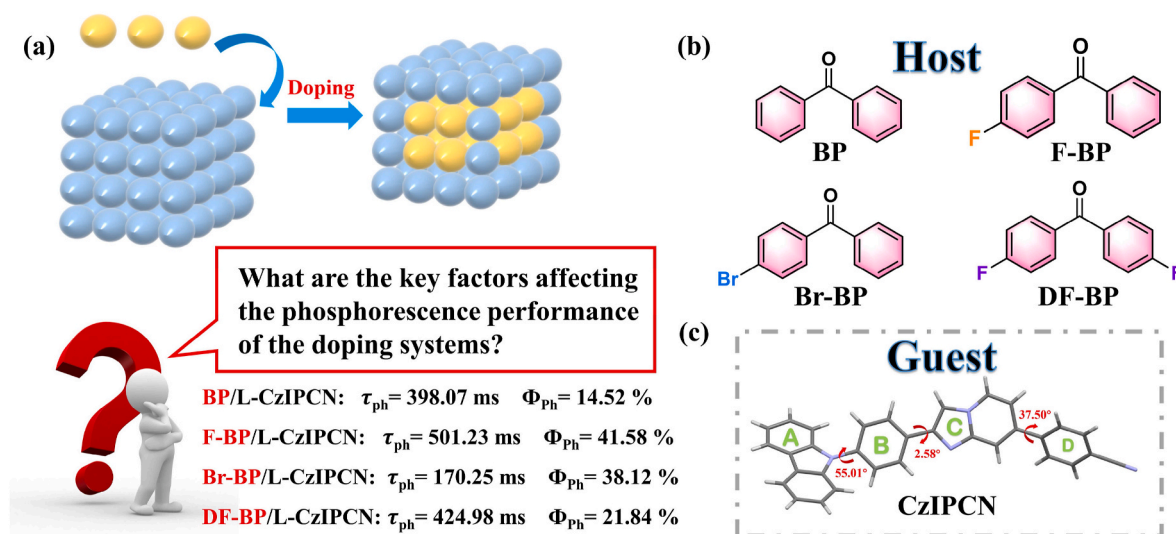
By slow solvent diffusion of n-hexane into CH_2Cl_2 solution of CzIPCNC at room temperature, yellow crystals CzIPCNC (CCDC 2270670) were obtained, indicating twisted molecular configuration, with dihedral angles of 55.01° , 2.58° and 37.50° for ring A-B, B-C and C-D respectively (Scheme 1c). To construct novel host-guest doping systems and explore the internal mechanism of RTP, a twisted D (carbazole unit)- π -A (cyanimidazopyridine unit) luminogens named as L-CzIPCNC was designed and synthesized by choosing self-made carbazole as raw material (Scheme 1), while CzIPCNC as a control was prepared by commercial carbazole. Compared with L-CzIP and CzIP [40], L-CzIPCNC and CzIPCNC should have smaller ΔE_{ST} due to the introduction of -CN. Then, host-guest doping systems were constructed by choosing L-CzIPCNC and CzIPCNC as guest materials, as well as polymethyl methacrylate (PMMA), polyvinyl alcohol (PVA), and a series of benzophenones with tiny structural differences as host materials. Subsequently, RTP performance of the host-guest doping systems were optimized by changing the doping ratios between host and guest materials. Although no visible afterglow can be observed with the naked eye without professional equipment for crystals L-CzIPCNC and CzIPCNC at room temperature, 0.2 % L-CzIPCNC@PMMA film (weight ratio of L-CzIPCNC and PMMA = 1:500) has RTP lifetimes of

102.73 ms and afterglow lifetimes of about 0.8 s after UV photo-radiation of 60 s. More excitingly, RTP and afterglow lifetimes of F-BP/L-CzIPCNC doping system (weight ratio of L-CzIPCNC and F-BP = 1:100) are up to 501.23 ms and over 4 s respectively, with a high RTP quantum yield of 41.58 %, which are significantly better than RTP and afterglow lifetimes of L-CzIP in the doping systems. Interestingly, L-CzIPCNC@PMMA film shows a single phosphorescence peak at near 505 nm, while BP/L-CzIPCNC, F-BP/L-CzIPCNC, Br-BP/L-CzIPCNC and DF-BP/L-CzIPCNC present dual-band RTP emission at near 550 nm and 600 nm, but different RTP lifetimes (170.25–501.23 ms) and afterglow (1.5–4 s). Different from previous reports, CzIPCNC shows similar RTP spectra (515 nm) and lifetimes (161.15 ms) to L-CzIPCNC in the corresponding PMMA films. By photophysical property tests and theoretical calculation, the intrinsic mechanism behind RTP were further discussed in detail. Finally, high-level anti-counterfeiting and encryption patterns were constructed based on different host-guest doping systems. It is worth mentioning that F-BP/L-CzIPCNC doping system combines long RTP lifetime and high quantum yield, which is very precious for pure organic RTP systems.

2. Results and discussion

2.1. Photo-physical properties in solution

L-CzIPCNC and CzIPCNC were carefully purified by column chromatography and slow diffusion of n-hexane into DCM solution of L-CzIPCNC/CzIPCNC. Then, L-CzIPCNC and CzIPCNC were characterized by ^1H and ^{13}C nuclear magnetic resonance (NMR) spectroscopies and high-resolution mass spectrum (HRMS). In the molecular skeleton of L-CzIPCNC, carbazole unit and cyanimidazopyridine unit serve as electron donor and electron acceptor respectively, which is linked by a benzene bridge, forming twisted molecular configurations, and reducing ΔE_{ST} . Besides, N atoms on conjugated heterocycles are expected to boost ISC. As shown in Fig. S1, with increasing of solvent polarity, absorption maxima of L-CzIPCNC show tiny red shifts, but its emission maxima shift to 470 nm from 386 nm, indicating obvious intramolecular charge transfer (ICT) characteristic. Molecular orbital amplitude plots of the highest occupied molecular orbital (HOMO) and lowest unoccupied molecular orbital (LUMO) levels further confirm ICT characteristic of L-CzIPCNC, whose HOMO orbitals mainly located at N-phenylcarbazole unit, but LUMO orbitals located at the remaining parts beyond the carbazole unit (Fig. S2). Noteworthy, CzIPCNC and L-CzIPCNC present the same absorption and emission spectra in DCM solution (Fig. S3),



Scheme 1. (a) Conceptual diagram, RTP lifetimes and quantum yields (Φ_{ph}) of four doping systems. (b) Molecular structures of four host materials (c) The molecular structure and conformation of CzIPCNC in crystalline state.

indicating the negligible influence of trace Bd.

2.2. Host-guest doping

Switching off UV lamp, L-CzIPCN emits bright orange afterglow in DCM solution at 77 K, but not for its crystals at room temperature (Fig. S4). The results indicate L-CzIPCN is a phosphor in nature, but crystalline samples cannot suppress non-radiative deactivation of triplet excitons at room temperature. To avoid complex crystal growth conditions and enhance the stability of triplet excitons, polymer matrix such as PVA and PMMA are usually chosen as host materials to inhibit molecular motion and oxygen diffusion. Here, host-guest doping systems were constructed and optimized by dissolving L-CzIPCN and PMMA/PVA at weight ratio of 1: 1000, 1: 500, 1:100 and 1:10, thereby causing a gradient of fluorescence emission from blue to pink in PMMA matrix, as well as from deep-blue to light-blue in PVA matrix with the increase of doping concentration of L-CzIPCN (Fig. 1a and Fig. S8). The corresponding emission maxima red shift to 440 nm from 410 nm due to ICT characteristic in PMMA matrix (Fig. 1b), as well as enhanced intermolecular stacking, and interactions, indicating doping concentration dependent fluorescence emission. Different from fluorescence emission, a series of L-CzIPCN@PMMA films generate a stable phosphorescent emission peak at 505 nm, indicating locally excited (LE) triplet state attributes. L-CzIPCN@PMMA films are irradiated by UV light for 1–5 s, no afterglow can be perceived by the naked eyes, whose RTP lifetimes are only 47.62–55.20 μ s (Fig. 1c). After exposure time is extended to 60 s, afterglow and RTP lifetimes of L-CzIPCN@PMMA films increase separately to 0.2–0.8 s and 61.89–102.73 ms (Fig. 1d), demonstrating RTP performance of L-CzIPCN. According to previous research results, the above phenomenon is attributed to the inability of PMMA to inhibit the diffusion of oxygen and the conversion of oxygen into singlet oxygen after UV radiation. Among of the PMMA films, 0.2 % L-CzIPCN@PMMA film gives the longest RTP lifetime and afterglow (Fig. 1 and Table S2), whose Φ_{ph} of 4.28 % is only second to that of 1 % L-CzIPCN@PMMA (5.42 %). Interestingly, the corresponding 0.2 % CzIPCN@PMMA film also exhibits the same RTP spectra without characteristic peaks of Bd

derivatives at near 570 nm and 600 nm (Figs. S5–6). However, 2 % CzIPCN@PMMA film compared with 0.2 % L-CzIPCN@PMMA film offers longer RTP lifetime (161.15 ms) and afterglow (2 s) after UV radiation of 60 s (Fig. S6), and the possible reason is that extremely trace amounts Bd derivatives still exist in CzIPCN after multi-step reaction and purification. By comparison, CzIPCN@PMMA film shows higher Φ_{ph} (6.56 %) than 1 % CzIP@PMMA film (Φ_{ph} = 3.76 %), as well as almost twice RTP lifetime and afterglow, confirming the rationality of introducing CN. By and large, fluorescence emission maxima show obvious bathochromic-shifts for L-CzIPCN@PVA films than the corresponding L-CzIPCN@PMMA films (Fig. 1b and Fig. S7). More importantly, RTP lifetime (221.66 ms) and afterglow (6 s) of 0.2 % L-CzIPCN@PVA film show significant increases compared with that of 0.2 % L-CzIPCN@PMMA film, which should be attributed to stronger intermolecular hydrogen bonds in PVA matrix. Of note, phosphorescence spectra of L-CzIPCN@PVA films present two emission peaks at 470–510 nm and 550–590 nm when the doping concentrations of L-CzIPCN are 0.1 %, 0.2 % and 1 %, but with a single emission peak at the doping concentrations of 10 %, which should be attributed to multiple different luminescence centers due to the uneven dispersion of hydrophobic L-CzIPCN in hydrophilic PVA films (Figs. S7–9 and Table S3). Compared Fig. S10b with Fig. S11, phosphorescence spectra of 0.2 % CzIPCN@PVA film show characteristic peaks of Bd at 570 nm and 620 nm when the delayed time is prolonged to 30 ms from 1 ms, confirming the presence of Bd or Bd derivatives in CzIPCN samples.

To obtain URTP materials and explore RTP mechanism of host-guest doping, benzophenone derivatives (BP, F-BP, Br-BP, and DF-BP) were chosen as hosts due to good crystallinity, similar structure, $n-\pi$ transition characteristic and low melting point. The doping systems with different molar ratios between guest and host were constructed by melting method, thereby the crystallinity of host materials was reserved, and RTP performance of the doping systems were optimized. Generally, doping concentration dependent phosphorescence performance is attributed to the inability of low concentration guests to form more triplet excitons, while excessive triplet excitons are prone to collision quenching. The doping results indicate that the doping systems with a

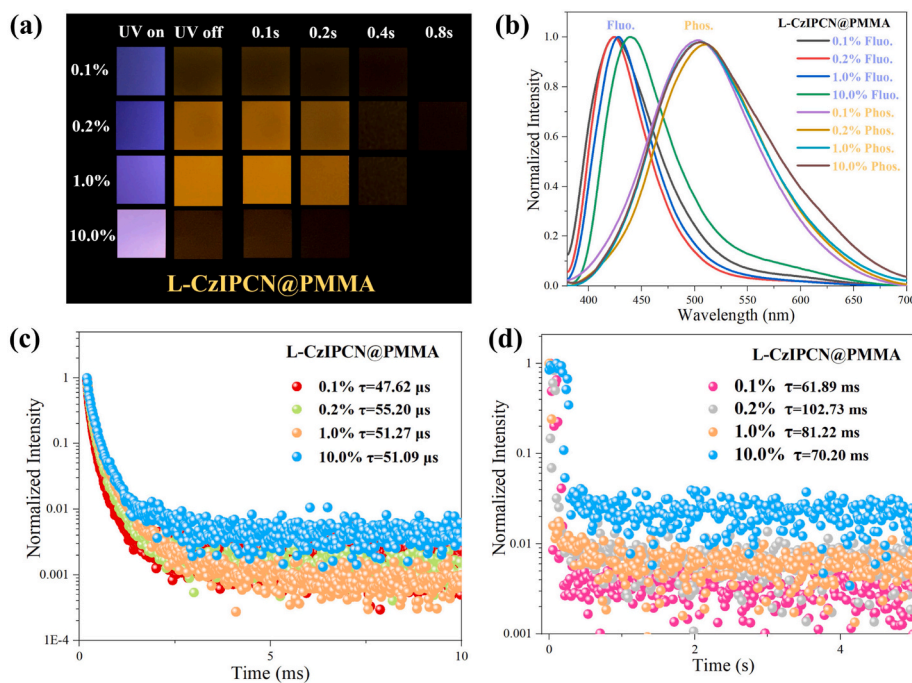


Fig. 1. (a) Photograph of L-CzIPCN@PMMA films under 365 nm UV light. (b) Fluorescence and phosphorescence spectra of L-CzIPCN@PMMA films at different doping concentrations (delayed time = 1 ms) (c). Time-resolved phosphorescence decay curves of L-CzIPCN@PMMA films excited at 365 nm (365 nm UV radiation for 1–5 s before testing). (d) Time-resolved phosphorescence decay curves of L-CzIPCN@PMMA films excited at 365 nm (365 nm UV radiation for 60 s before testing).

host-guest molar ratio of 100:1 show the strongest RTP emission (Fig. S12), whose luminescence characteristics are systematically investigated without further explanation in the following. Four doping systems exhibit a wide emission band (400–680 nm) with an emission peak of approximately 440 nm, but they present different colors under UV radiation due to different intensity ratios between 400–500 nm and 500–680 nm (Fig. 2a and b). By contrast, Br-BP/L-CzIPCN show two obvious emission peaks at 555 nm and 600 nm in fluorescence spectra, which are the same as emission maxima of RTP, condignly coming from triplet excitons, but similar long wavelength emission peaks cannot be found in the other three doping systems. Considering the heavy atom effect of bromine atom, the above differences should be due to the enhanced phosphorescence radiation rate and SOC between singlet (S_n) and T_n . The four host-guest doping systems all emit a strong orange afterglow after switching off the UV light and F-BP/L-CzIPCN doping system shows the longest phosphorescence lifetime (501.23 ms) and afterglow (4 s) (Fig. 2c), as well as the highest RTP quantum yield, followed by Br-BP/L-CzIPCN, DF-BP/L-CzIPCN and BP/L-CzIPCN. To eliminate the influence of delayed spectra of benzophenone derivatives at 400–500 nm, quantum yields of four host-guest doping systems were tested by increasing the delay time to 30 ms. Br-BP/L-CzIPCN gives the highest RTP quantum yield, followed by F-BP/L-CzIPCN, DF-BP/L-CzIPCN, and BP/L-CzIPCN. For Br-BP/L-CzIPCN, the high RTP quantum yield, short RTP lifetime and afterglow should be due to heavy-atom effect. Compared with PMMA, the benzophenone derivatives can more effectively restricted oxygen diffusion and guest molecular motion, leading to more persistent RTP for DF-BP/L-CzIPCN, BP/L-CzIPCN, F-BP/L-CzIPCN and Br-BP/L-CzIPCN than 0.2 % L-CzIPCN@PMMA film. What's particularly interesting is all the doping systems show two phosphorescence emission peaks at near 550 nm and 600 nm (Fig. 2a), further confirming LE triplet state attributes of L-CzIPCN. L-CzIPCN shows different RTP in benzophenone derivatives and PMMA films, which may be attributed to different host-guest interactions and variable molecular conformation for L-CzIPCN [41,42]. As documented, some doping systems constructed from benzophenone derivatives exhibit phosphorescence spectra and emission peaks similar to that of BP/L-CzIPCN, but the corresponding guest materials have completely

different molecular structures with L-CzIPCN [43]. To ascertain the reasons behind the above problem, phosphorescence spectra of L-CzIPCN were recorded in DCM solution at 77 K, which also presented dual band phosphorescence emission at 550 nm and 606 nm, demonstrating RTP of the doping systems derived from guest monomers (Fig. S14), as well L-CzIPCN was evenly dispersed in host materials. Furthermore, the delayed phosphorescence spectra of four host materials give similar multiple emission peaks located at 400–700 nm (Fig. S20b). Obviously, phosphorescence spectra between host and their doping systems are inconsistent, excluding RTP of the doping systems from host again.

2.3. Phosphorescence mechanism of host-guest doping

Taking F-BP/L-CzIPCN as an example, UV-Vis absorption spectra of the doping system contains two absorption bands (Fig. 3a), located at 250–300 nm and 300–550 nm, respectively. Compared with F-BP and L-CzIPCN, the F-BP/L-CzIPCN doping system does not produce new absorption peaks, eliminating the formation of exciplex. Noteworthy, there is some overlap between the emission spectrum of F-BP and the absorption spectrum of L-CzIPCN at 370–410 nm (Fig. 3b), which may trigger Förster resonance energy transfer (FRET). Thereby, phosphorescence intensity of F-BP/L-CzIPCN at different excitation wavelength were provided, which indicated the strongest phosphorescence intensity at 365 nm excitation, followed by 420 nm and 285 nm (Fig. 3c). Combined with lower absorption intensity at 420 nm compared to 280 nm for F-BP, it can be inferred that phosphorescence of F-BP/L-CzIPCN should be excitation of guest, but not for FRET. The remaining three groups of doped systems also exhibited similar spectral phenomena (Figs. S16–S18).

To further make clear RTP mechanism of the doping systems, the energy levels, SOC coefficients (ξ), dipole moments, and molecular orbitals of four hosts were calculated by using time-dependent density functional theory (TD-DFT) calculations at the B3LYP/6-31G(d). Br-BP and F-BP show obvious electron density migration from HOMO to LUMO, indicating typical charge transfer (CT) excitation, while HOMO and LUMO of BP and DF-BP located on the whole molecule, without an

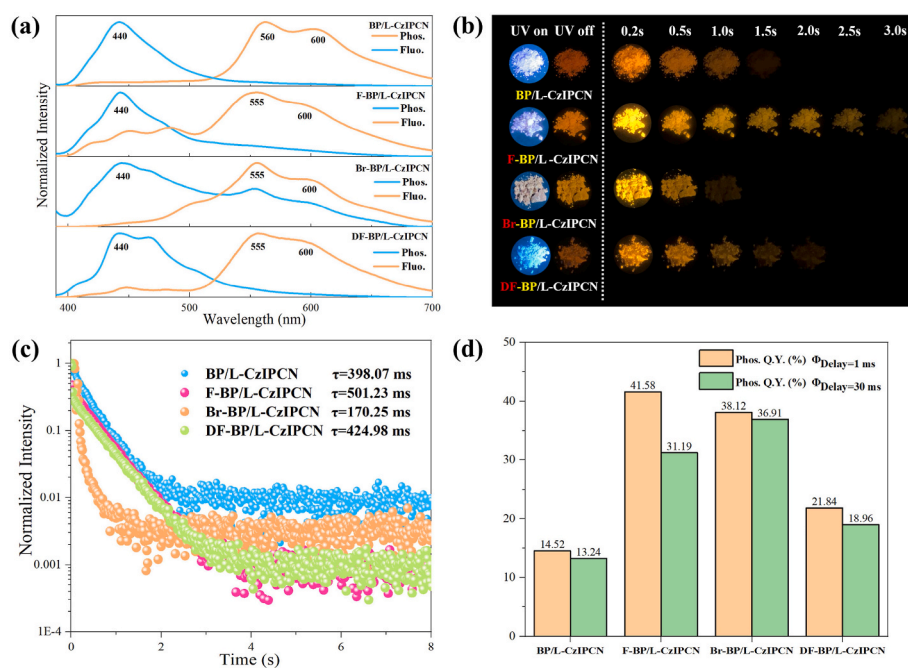


Fig. 2. (a) Transient fluorescence and delayed phosphorescence spectra of four doping systems (delayed time = 1 ms). (b) Photographs of four host-guest doping systems by turning on-off 365 nm lamp. (c) Time-resolved phosphorescence decay curves of four doping systems ($\lambda_{ex} = 365$ nm). (d) Φ_{ph} of four doping systems (delayed time = 1 ms and 30 ms.).

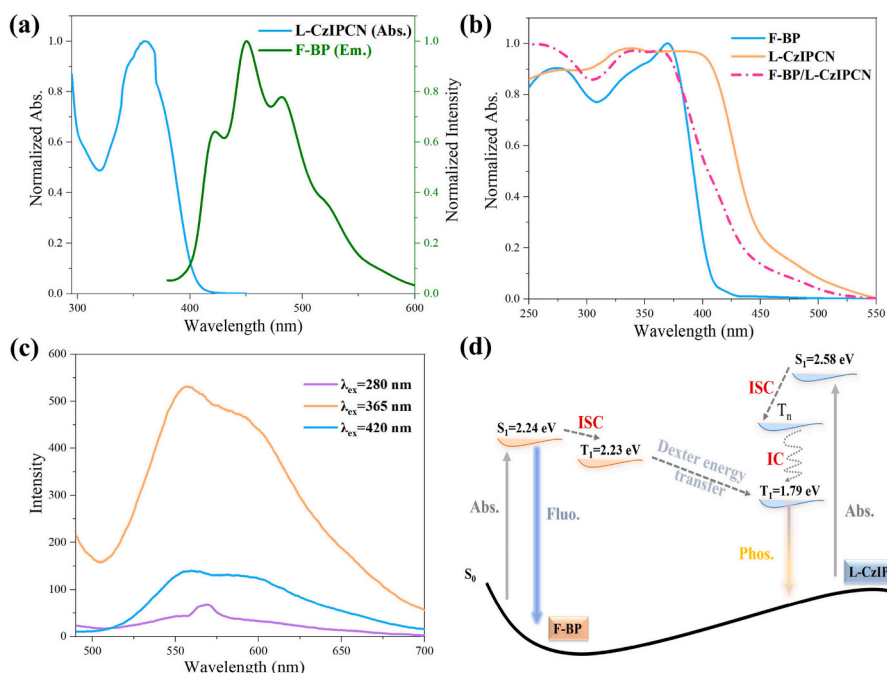


Fig. 3. (a) UV-Vis absorption spectra of F-BP, L-CzIPCN and F-BP/L-CzIPCN in solid states. (a) Fluorescence spectra of F-BP in solid states and UV-Vis absorption spectra of L-CzIPCN in dichloromethane solution (1×10^{-5} M). (c) Delayed phosphorescence spectra of F-BP/L-CzIPCN at different excitation wavelengths. (d) Proposed photophysical processes in F-BP/L-CzIPCN doping system.

obvious CT excitation (Fig. 4a). As documented [44], CT excitation is beneficial for reducing the energy level of S_1 , which is consistent with the smaller S_1 for Br-BP and F-BP than BP and DF-BP (Fig. 4b). Furthermore, T_1 energy levels of the four host materials are basically constant, which sandwich between S_1 and T_1 levels of L-CzIPCN, facilitating rapid ISC of L-CzIPCN. Compare L-CzIPCN with L-CzIP, ΔE_{ST} is reduced to 0.79 eV from 1.13 eV after the introduction of CN (Fig. S21). Meanwhile, there are three triplet excited states (T_2 , T_3 and T_4) around the S_1 state of L-CzIPCN, which can promote the rapid generation of triplet excitons due to appropriate ξ ($S_1 \rightarrow T_2 = 0.337 \text{ cm}^{-1}$, $S_1 \rightarrow T_3 = 0.102 \text{ cm}^{-1}$ and $S_1 \rightarrow T_4 = 0.099 \text{ cm}^{-1}$) and tiny energy gaps ($\Delta E_{S_1T_2} = 0.21 \text{ eV}$, $\Delta E_{S_1T_3} = 0.21 \text{ eV}$, and $\Delta E_{S_1T_4} = 0.34 \text{ eV}$). Besides, the dipole-dipole interactions between guest with ICT effect and host can lower the energy level of S_1 state of guest but hardly have influence on the energy level of T_1 state of guest, leading to the decrease of ΔE_{ST} of guest [45]. Moreover, the larger the dipole moment of host, the more significant the decrease in ΔE_{ST} . The calculated results indicate the dipole moments of DF-BP, Br-BP, BP, and F-BP increase from 1.83 D, 2.84 D, 3.06 D to 3.19 D in sequence, and thereby F-BP possesses

advantages over the other hosts in reducing ΔE_{ST} of L-CzIPCN. Furthermore, F-BP has the smallest ΔE_{ST} , followed by Br-BP, BP, and DF-BP. Large dipole moment and small ΔE_{ST} play an important role in boosting ISC processes, and thus produce higher Φ_{ph} for F-BP/L-CzIPCN doping system. Meanwhile, F-BP/L-CzIPCN gives the smallest non-radiative rate (k_{phnr}) and decent RTP radiation rate (K_{ph}), thereby yielding the longest RTP lifetime and afterglow (Table S4). For comparison, DF-BP and BP have equivalent ΔE_{ST} (0.69 eV and 0.68 eV) and ξ (12.12 cm^{-1} and 14.12 cm^{-1}), while the latter has a bigger dipole moment. Based on ΔE_{ST} , ξ and dipole moment, BP/L-CzIPCN should show higher inter-system transition rate (K_{ISC}) compared with DF-BP/L-CzIPCN, which is consistent with experimental results (Table S4). However, BP/L-CzIPCN shows inferior Φ_{ph} and RTP lifetime than DF-BP/L-CzIPCN due to the increased k_{phnr} and reduced K_{ph} . Br-BP/L-CzIPCN has the highest K_{ISC} and K_{ph} because of the heavy atom effect, leading to the shortest RTP lifetime. Based on theoretical calculations and the above analysis, taking F-BP/L-CzIPCN as an example, the corresponding phosphorescence emission mechanism is outlined (Fig. 3d). Under ultraviolet radiation of 365 nm, F-BP and L-CzIPCN

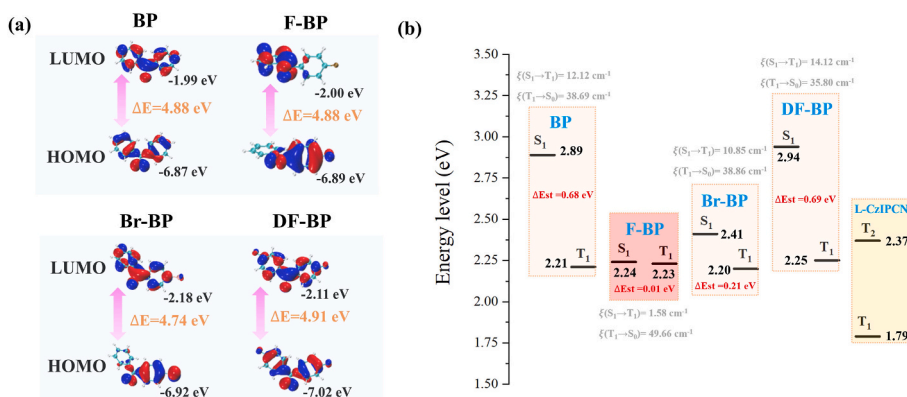


Fig. 4. (a) Molecular orbital amplitude plots of HOMO and LUMO levels for BP, F-BP, Br-BP, and DF-BP. (b) The single-molecule energy level diagrams and SOC coefficient between S_1 and T_1 for BP, F-BP, Br-BP, and DF-BP.

transition to S_1 state from S_0 state. Then S_1 excitons of L-CzIPCN transfer to its T_2 , T_3 and T_4 states by ISC. Subsequently, they relax to T_1 state of L-CzIPCN, and then T_1 excitons backs to S_0 state, emitting RTP of L-CzIPCN. Owing to large $\xi(S_1 \rightarrow T_1)$ and tiny ΔE_{ST} , S_1 excitons of F-BP rapidly transfer to its T_1 state, and then transfer to T_1 state of L-CzIPCN by Dexter energy transfer (DET) process, generating RTP of L-CzIPCN after ISC of $T_1 \rightarrow S_0$.

3. Applications

Based on excellent luminescence and ultra-long RTP lifetime of four doping systems, a series of anti-counterfeiting patterns and information encryption were designed and drawn by DCM solution of L-CzIPCN on filter papers soaked with different host materials. Fig. 5a shows that four blue pandas with different postures are clearly visible under UV irradiation of 365 nm, but they are invisible in sunlight due to weak absorption in the visible light region for host-guest doping systems. After removing the UV lamp, blue pandas turn into bright yellow pandas, and the various complex patterns present good resolution. A higher level of encryption was completed by selecting BP/L-CzIPCN and F-BP/L-CzIPCN doping systems, which had similar fluorescence and RTP emission but different afterglow lifetime. As shown in Fig. 5b, “UO” and “RTP” were written by using BP/L-CzIPCN and F-BP/L-CzIPCN doping systems respectively, which displayed blue “UORTP” when UV lamp of 365 nm was switched on. When UV lamp of 365 nm was switched off, yellow “UORTP” as a false information was presented. After 1 s, only “RTP” as a true information could be perceived. It is worth noting that forgery of document, certificate and banknote deeply affects the information security of individuals and even the whole country, thus it is becoming increasingly important to develop safe inks that cannot be copied but can only be read under special conditions. We know that ordinary documents are often printed on the A4 paper, thereby a encrypt document is constructed by adopting F-BP/L-CzIPCN doping system and a piece of A4 paper containing printed text. Except for the printed text, no other trace can be observed in sunlight, and the flexibility of A4 paper is not affected after soaking of molten F-BP (Fig. 5c). Owing to the strong fluorescence emission inherent for A4 paper, encrypted information still cannot be observed under UV radiation of 365 nm. After turning off UV

lamp, yellow “RTP” is clearly visible. The above results indicate that the doping systems can effectively encrypt information and draw anti-counterfeiting patterns on papers and documents, but it must be pointed out that all paper used for writing patterns and text must undergo soaking treatment.

4. Conclusions

In summary, L-CzIPCN and CzIPCN with D- π -A molecular configuration were prepared by using carbazole synthesized in the laboratory and commercial carbazole, and characterized by ^1H NMR, ^{13}C NMR and HR-MS. L-CzIPCN and CzIPCN present the same UV-vis absorption and fluorescence emission spectra, as well as phosphorescence spectra in DCM solution at 77 K, indicating negligible influence for trace Bd. Compared with L-CzIP, L-CzIPCN shows smaller ΔE_{ST} and more ISC channels by the introduction of CN. A series of new host-guest doping systems were developed by adopting L-CzIPCN/CzIPCN and PMMA/dibenzophenone derivatives as guests and hosts respectively. 0.2 % L-CzIPCN@PMMA film shows photo-radiation dependent phosphorescence lifetime and slightly shorter RTP lifetime compared with that of 0.2 % CzIPCN@PMMA, which are attributed to the residual oxygen in PMMA film and extremely trace amounts Bd in CzIPCN separately. Different from 0.2 % L-CzIPCN@PMMA film, F-BP/L-CzIPCN, DF-BP/CzIPCN, BP/CzIPCN and Br-BP/CzIPCN have dual-band RTP emission at 550 nm and 600 nm, which are designated as the phosphorescence of the guest monomers, indicating that L-CzIPCN is well dispersed in benzophenone derivatives. Among of four benzophenone derivatives doped systems, F-BP/L-CzIPCN shows the longest phosphorescence lifetime (501.23 ms) and afterglow (4 s), as well as higher quantum yield (31.19 %) due to the minimum ΔE_{ST} and the maximum dipole moment, while Br-BP/L-CzIPCN gives the shortest phosphorescence lifetime because of heavy-atom effect. DF-BP relative to BP has equivalent ΔE_{ST} and ξ , as well as smaller dipole moment. From this, longer RTP lifetime and quantum efficiency for DF-BP/L-CzIPCN than BP/L-CzIPCN may be attributed to stronger intermolecular interactions for DF-BP than BP. Overall, the benzophenone derivatives have excellent crystallinity and large ξ ($S_1 \rightarrow T_1$), and T_1 states of the benzophenone derivatives can act as an energy bridge between S_1 and T_1 states of L-CzIPCN, which



Fig. 5. (a) Anti-counterfeiting patterns constructed by four doping systems. (b) Text encryption based on BP/L-CzIPCN and F-BP/L-CzIPCN. (c) Encryption application of F-BP/L-CzIPCN on A4 paper.

significantly improve RTP performance of L-CzIPCN. Owing to excellent luminescence and different RTP lifetimes, four benzophenone derivatives/L-CzIPCN doping systems can be used as high-level anti-counterfeiting and information encryption materials. The work not only provides a series of new host-guest doping systems, but also provide some valuable guidance for further optimization of host-guest doping systems and molecular design.

CRediT authorship contribution statement

Jianfeng Jiang: Writing – original draft, Data curation. **Jiaqi Liu:** Data curation. **Chenwei Hu:** Data curation. **Yongtao Wang:** Writing – original draft, Conceptualization. **Lei Ma:** Data curation.

Declaration of competing interest

There are no conflicts to declare.

Data availability

No data was used for the research described in the article.

Acknowledgments

This work was supported by the Guangxi Natural Science Foundation (Grant No. 2020GXNSFAA159147), and the National Natural Science Foundation of China (Grant No. 21766030 and 21566034).

Appendix A. Supplementary data

Supplementary data to this article can be found online at <https://doi.org/10.1016/j.dyepig.2023.111931>.

References

- [1] Yan X, Peng H, Xiang Y, Wang J, Yu L, Tao Y, Li H, Huang W, Chen R. *Small* 2022;1(18):2104073.
- [2] Cai S, Yao X, Ma H, Shi H, An Z. *Aggregate* 2023;3(4):e320.
- [3] Shi H, Yao W, Ye W, Ma H, Huang W, An Z. *Acc Chem Res* 2022;23(55):3445–59.
- [4] Zhao W, He Z, Tang BZ. *Nat Rev Mater* 2020;12(5):869–85.
- [5] Wang X, Wang Z, Feng H, Lin C, Shi H, An Z, Su Z-M, Liang F-S. *Chem Commun* 2022;22(58):3641–4.
- [6] Shan H, Liu A, Lv Y, Wu X, Ma Y, Jin X, Guo J. *Dyes Pigments* 2020;180:108400.
- [7] Ren J, Tian Y, Wang Y, Yang J, Fang M, Li Z. *J Mater Chem C* 2022;37(10):13741–6.
- [8] Huang Y, Zheng X, Yao Z, Lv W, Xiang S, Ling Q, Lin Z. *Chem Eng J* 2022;444:136629.
- [9] Yang Z, Mao Z, Zhang X, Ou D, Mu Y, Zhang Y, Zhao C, Liu S, Chi Z, Xu J. *Angew. Chem.-Int. Edit.* 2016;6(128):2221–5.
- [10] Xu W, Yu Y, Ji X, Zhao H, Chen J, Fu Y, Cao H, He Q, Cheng J. *Angew. Chem.-Int. Edit.* 2019;45(131):16164–8.
- [11] Lu Y, Chen X, Suh YD, Liu X, Huang W. *Adv Opt Mater* 2023;2300240.
- [12] Cong Z, Han M, Fan Y, Fan Y, Chang K, Xiao L, Zhang Y, Zhen X, Li Q, Li Z. *Mater Chem Front* 2022;12(6):1606–14.
- [13] Xiao G, Ma Y-J, Fang X, Yan D. *ACS Appl Mater Interfaces* 2022;26(14):30246–55.
- [14] Hao W, Li Y, Liu M. *Adv Opt Mater* 2021;15(9):2100452.
- [15] Zhou B, Qi Z, Yan D. *Angew. Chem.-Int. Edit.* 2022;39(61):e202208735.
- [16] Ni Y, Yang L, Kong L, Wang C, Zhang Q, Yang J. *Mater Chem Front* 2022;23(6):3522–30.
- [17] Zhang X, Qian C, Ma Z, Fu X, Li Z, Jin H, Chen M, Jiang H, Ma Z. *Adv Sci* 2023;3(10):2206482.
- [18] Guo Y, Chen K, Hu Z, Lei Y, Liu X, Liu M, Cai Z, Xiao J, Wu H, Huang X. *J Phys Chem Lett* 2022;32(13):7607–17.
- [19] Xiao F, Gao H, Lei Y, Dai W, Liu M, Zheng X, Cai Z, Huang X, Wu H, Ding D. *Nat Commun* 2022;13(1):186.
- [20] Deng J, Guan Z, Fu D, Zheng Y, Chen Z, Li H, Liu X. *Adv Opt Mater* 2023;2300207.
- [21] Kong L, Zhu Y, Sun S, Li H, Dong S, Li F, Tao F, Wang L, Li G. *Chem Eng J* 2023;143931.
- [22] Xu X, Zhang W, Liu M, Lei Y, Zhou Y, Guan Y, Huang X, Wu H. *Adv Opt Mater* 2023;2300284.
- [23] Chen L, Zhao S, Wang Y, Yu S, Yang Y, Liu X. *Sensor Actuator B Chem* 2023;390:133946.
- [24] Wang J, Li N, Yang X-Q, Wang L-L, Ni R-Y. *Dyes Pigments* 2022;207:110732.
- [25] Chen J, Zhang Y, Zhang S, Liu G, Sun Q, Xue S, Yang W. *Small Struct* 2023;2300101.
- [26] Wu Z, Nitsch J, Marder TB. *Adv Opt Mater* 2021;20(9):2100411.
- [27] Li Z, Cao M, Rao Z, Zhao X, Gong X. *Small* 2023;2302357.
- [28] Yang L, Wang X, Zhang G, Chen X, Zhang G, Jiang J. *Nanoscale* 2016;40(8):17422–6.
- [29] Sun H, Wei X, He Y, Xiao Y, Wu Y, Xie Z, et al. *Mater Chem Front* 2023;7(15):3156.
- [30] Zhang Y, Zhang S, Liu G, Sun Q, Xue S, Yang W. *Chem Sci* 2023;19(14):5177–81.
- [31] Sun J, Qian C, Ma Z, Wang S, Ma Z. *Dyes Pigments* 2022;201:110196.
- [32] Chen C, Chi Z, Chong KC, Batsanov AS, Yang Z, Mao Z, Yang Z, Liu B. *Nat Mater* 2021;2(20):175–80.
- [33] Chen X, Dai W, Wu X, Su H, Chao C, Lei Y, Shi J, Tong B, Cai Z, Dong Y. *Chem Eng J* 2021;426:131607.
- [34] Xu X, Chen Z, Lei Y, Sun X, Liu M, Wu H, Huang X. *Chem Commun* 2022;79(58):11143–6.
- [35] Yang J, Wu X, Shi J, Tong B, Lei Y, Cai Z, Dong Y. *Adv Funct Mater* 2021;52(31):2108072.
- [36] Gao M, Tian Y, Li X, Gong Y, Fang M, Yang J, Li Z. *Angew. Chem.-Int. Edit.* 2023;5(135):e202214908.
- [37] Qiu W, Cai X, Li M, Chen Z, Wang L, Xie W, Liu K, Liu M, Su S-J. *J Phys Chem Lett* 2021;19(12):4600–8.
- [38] Yue L, Yuan S, Zhang Y, Wang Y, Sun Q, Zhang H, Xue S, Yang W. *J Phys Chem Lett* 2021;47(12):11616–21.
- [39] Ding S, Xu Y, Li J, Wang X, Wang G, Li H, Ren S, Zhang K. *Dyes Pigments* 2023;210:110984.
- [40] Jiang J, Hu C, Wang Y, Ma L, Guo J. *Mater Today Chem* 2023;(30):101548.
- [41] Gao M, Ren J, Gong Y, Fang M, Yang J, Li Z. *Aggregate* 2023;(462):1.
- [42] Li D, Han Y, Jiang Y, Jiang G, Sun H, Sun Z, Zhang Qi, Tian Y. *ACS Appl Mater Interfaces* 1807;(14):2022.
- [43] Guo Y, Wang Y, Gao Y, Zhang J, Wang C, Zhao G. *J Ind Eng Chem* 2023;120:140–6.
- [44] Chen Y, Xie Y, Shen H, Lei Y, Zhou Y, Dai W, Cai Z, Liu M, Huang X, Wu H. *Chem Eur J* 2020;72(26):17376–80.
- [45] Li J, Wang G, Chen X, Li X, Wu M, Yuan S, Zou Y, Wang X, Zhang K. *Chem Eur J* 2022;35(28):e202200852.